



Mono Lacunary Phosphotungstate Loaded Zeolite HY For the Esterification of Levulinic and Succinic Acid Into Fuel Additives

Anjali Patel¹ · Margi Joshi¹

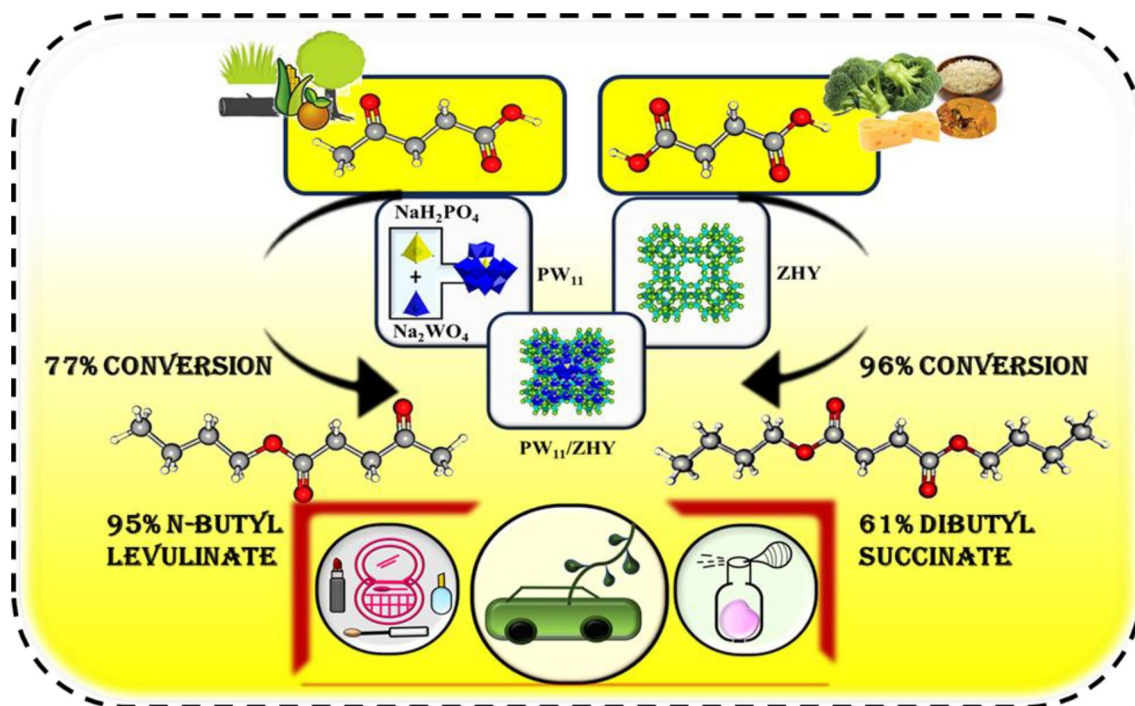
Received: 19 March 2024 / Accepted: 15 July 2024

© The Author(s), under exclusive licence to Springer Science+Business Media, LLC, part of Springer Nature 2024

Abstract

The legal obligation to swiftly adopt renewable energies has been increased because of the continuous usage of fossil fuels. In this perspective, biomass serves as a pillar to improve the current conditions over different heterogeneous catalysts due to their known advantages. This work is focused on the synthesis of a novel catalyst comprising mono lacunary phosphotungstate and zeolite HY. The catalyst was characterized by number of physicochemical techniques and evaluation of the activity of catalyst for the esterification of most promising bio platforms, levulinic acid and succinic acid to produce fuel additives. After a detailed optimization of both reactions, remarkable conversions of levulinic acid (77%) and succinic acid (96%) with turnover numbers of 2749 and 3427 respectively, were obtained. The order of the reaction and activation energy for the said reactions were calculated in the kinetic study. The sustainable nature of the catalyst was confirmed via regeneration and viability towards other bio-based molecules which enhances its industrial importance.

Graphical Abstract



Keywords Heterogeneous catalysis · Heteropoly acids · Zeolites · Mono lacunary phosphotungstate · Esterification · Bio platform molecules · Fuel additives

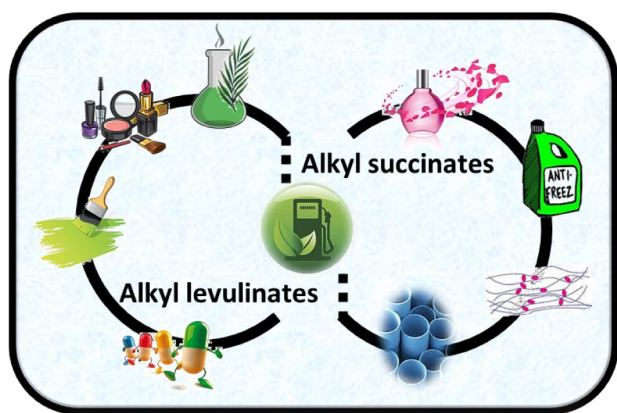
Extended author information available on the last page of the article

1 Introduction

Keggin type of polyoxometalates (POMs) have attracted much attention in the past two decades because of their unusual and desirable properties as well as potential applications, mostly centred on catalysis. Polyoxometalates have the general formula $[XM_{12}O_{40}]^{n-}$, where X stands for the heteroatom (P, Si or B in their higher oxidation states), M is the addenda atom (V, Mo or W all are in respective higher oxidation states), and O is for oxygen [1]. By introducing a structural defect, it is possible to design polyoxometalates at the molecular level, giving rise to Lacunary polyoxometalates (LPOMs), a well-known polyoxometalate family member. The wide range of structural configurations and unique electronic characteristics of lacunary polyoxometalates make them fascinating within the boundaries of current research paradigm. The development of lacunary polyoxometalates is quite simple and can be accomplished in one of two ways: either by condensation of individual metal salts or by removing one or more metal–oxygen (M–O) units from the parent Keggin anion in alkaline media, and are referred to as mono lacunary polyoxometalates or poly lacunary (di and tri) polyoxometalates accordingly [2, 3].

Like polyoxometalates, lacunary polyoxometalates provide contributions to the area of catalysis as they possess different structural combinations and special electronic properties. By means of this, mono lacunary phosphotungstate (PW_{11}) were explored in the various catalytic reactions in homogeneous medium, but it suffers from well-known drawbacks like confined stability, lower surface area, high solubility in polar solvents, and uneasy separation from the reaction mass. To navigate across these downsides, utilization of PW_{11} as a heterogeneous catalyst by anchoring onto multiple supports [4–19]. In 2015, TiO_2 supported potassium salt of mono lacunary phosphotungstate was synthesized for the photolytic conversion of glucose by E. I. García-López et al. [4]. Further, in the same year, A. Patel et al. synthesized a mono lacunary phosphotungstate anchored to MCM-41 and studied its catalytic activity in the transesterification of waste cooking oil for biodiesel production [5]. In 2016, the same group had developed catalysts for the oxidation of alkenes and alcohols that used mono lacunary phosphotungstate and two distinct types of mesoporous materials (MCM-41 and MCM-48) [6]. Again, the same group reported the oxidative esterification of benzaldehyde over ZrO_2 supported Cs-salt of mono nickel substituted phosphotungstate ($PW_{11}Ni/ZrO_2$) [7]. After that in the same year, Y. Wang et al. developed a catalyst via immobilization of sodium salt of mono lacunary phosphotungstate on quaternary ammonium functionalized chloromethylated polystyrene for oxidation of alcohols [8]. G. S. Armatas

et al. developed a synthesis of photocatalyst for hydrogen evolution made up of ordered mesoporous mono lacunary polyoxometalate–organosilica frameworks, in the same year [9]. In 2017, A. Patel et al. performed glycerol esterification as well as oxidation by using, mesoporous materials (MCM-41 and MCM-48) supported mono lacunary phosphotungstate [10]. In 2021, H. Zhang et al. developed a catalyst via immobilization of potassium salt of mono lacunary phosphotungstates on ZrO_2 nanofibers and used it in extraction catalytic oxidation desulfurization system [11]. In 2022, D. Contreras et al. reported tetra butyl ammonium (TBA) salts of Keggin-type polyoxoanions, $TBA_4PW_{11}V_1O_{40}$ for the selective aerobic oxidation of benzyl alcohol [12]. After, in the same year, C. N. Kato et al. explored the effect on sintering-resistance and photocatalysis by using a catalyst, two tungstates containing platinum nanoparticles (Pt Npts) that were obtained by air-calcining α -Keggin-type di platinum (II)-coordinated polyoxotungstates, $Cs_3[\alpha-PW_{11}O_{39}\{cis-Pt(NH_3)_2\}_2] \cdot 8H_2O$ [13]. The nano-sized organic–inorganic hybrid systems $(TBA)_7[PW_{11}O_{39}]$ as heterogeneous catalysts for the synthesis of phenyltrimethylsilyloxy-acetonitrile derivatives by using aldehydes and ketones by M. M Heravi et al. in the same year [14]. Further, V. S. Korenev et al. studied the azide coordination to polyoxometalates and synthesized $(Bu_4N)_{4.3}K_{0.7}[PW_{11}O_{39}Fe^{III}N_3] \cdot 2.5H_2O$ [15]. Recently in 2023, K. Shakeela and R. Shaikh et al. reported synthesis of cyclic carbonates by using hybrid materials of different metals (Cu^{2+} , Co^{2+} and Ni^{2+}) substituted phosphotungstates and poly (diallyldimethylammonium) chloride polymer (PDDA) [16]. Further, in the same year V. S. Korenev et al. reported the synthesis and characterization of these lanthanide complexes with mono lacunary phosphotungstates, $(Me_4N)_2K_2 [Gd (H_2O)_2PW_{11}O_{39}] \cdot 5H_2O$, $(Me_4N)_6K_2 [Gd (H_2O)_3PW_{11}O_{39}]_2 \cdot 20H_2O$, and $(Me_4N)_7 K [Gd (H_2O)_3PW_{11}O_{39}]_2 \cdot 12H_2O$ [17]. Again, in the same year H. Zheng et al. reported styrene epoxidation catalysed by $(MTOA)_7PW_{11}O_{39}$ which is made up of quaternary ammoniums and polyoxometalate [18]. Z. M. A. Merican et al. synthesized a series of POM@MOF nanocomposites made up of transition metals substituted Keggin-type PW_{11} and a zirconium-based MOF-808(Zr) for oxidative desulfurization of fuel oil [19]. It is worth mentioning that no available literature is on PW_{11} on to ZHY for biomass conversion, despite this, it offers numerous advantages, particularly in the areas of detergents, gas separation, desiccants, and catalysts. Zeolites' primary uses as catalysts, in which three distinct classes can be used to categorize the catalysis over zeolites: The three types of reactions are: 1) inorganic, 2) organic, and 3) hydrocarbon conversion. The catalytic features of zeolites include acidity, shape-selectivity, high surface area, and structural stability, among many other special qualities.



Scheme 1: Applications of alkyl levulinates and succinates

Scheme 1 Applications of alkyl levulinates and succinates

Amongst biomass conversion, Levulinic acid (C5), which ranks among the top twelve bio platform molecules, serves as a foundation for the investigation of further valuable chemicals, such as angelica lactones, 2-methyltetrahydrofuran, alkyl levulinates, succinic acid, γ -valerolactone, and pyrrolidines [20]. The alkyl levulinates are widely employed in the biofuel and fragrance industries. Amongst them, n-butyl levulinates are in the spotlight with their multiple applications such as in flavour-enhancing agents, food contact, cosmetics, polymer precursors, and most importantly of the recent trend, fuel additives [21].

At the same time, Succinic acid (C4), another important bio platform molecule, is an intriguing building block for a variety of industrial chemicals that could eventually take the place of maleic anhydride. Several routes including esterification, dehydration, dehydrogenation, amidation, hydrogenation, and polymerization were explored for the valorisation of succinic acid into value added products [22]. In the industrial sector, diesters of succinic acid are particularly popular due to their potential application as bio-based solvents, plasticizers, food preservatives, medicines, and cosmetics [23]. The schematic representation of their applications is shown in scheme 1.

Due to the importance of the said bio platform molecules, it was thought to investigate the esterification reaction of C4 and C5 acids with n-butanol in order to synthesize fuel additives under mild conditions.

This article describes the synthesis and detailed characterization of a novel heterogeneous catalyst comprising PW_{11} and ZHY. The catalyst was evaluated for the synthesis of fuel additives by the esterification of two major bio platform molecules, succinic acid and levulinic acid, with n-butanol. To achieve the maximum conversion as well as selectivity, experiments were carried out by varying number of reaction parameters (mole ratio, catalyst quantity,

temperature, and time). Further, kinetic study was carried out to determine the activation energy, and the capacity for recycling across numerous catalytic cycles was also investigated. The recovered and regenerated catalyst was explored for acidity measurement, FT-IR, TGA analysis and catalytic activity to show its sustainability. Further, the catalyst was evaluated to the esterification of various bio-based substrates to study its viability.

2 Experimental

2.1 Materials

All chemicals used were of A. R. grade. 12-Tungstophosphoric acid (extra pure), ammonium chloride (99%), n-butanol (>99%), 1-propanol (>99%), 1-pentanol (>99%), 1-hexanol (>99%), 1-heptanol (>99%), methanol (99%), ethanol (99%), dichloromethane (>99%), disodium hydrogen phosphate (>99%), sodium tungstate dihydrate (>99%), succinic acid (99.5%), were used as received from Merck. Levulinic acid (>98%) was acquired from Avra Synthesis Pvt. Ltd. Zeolite NaY was obtained commercially from Reliance Industries Limited, Vadodara, Gujarat.

2.2 Synthesis

Synthesis of the catalyst was carried out in three steps.

Step I: Conversion of NaY to its protonic form Zeolite HY (ZHY).

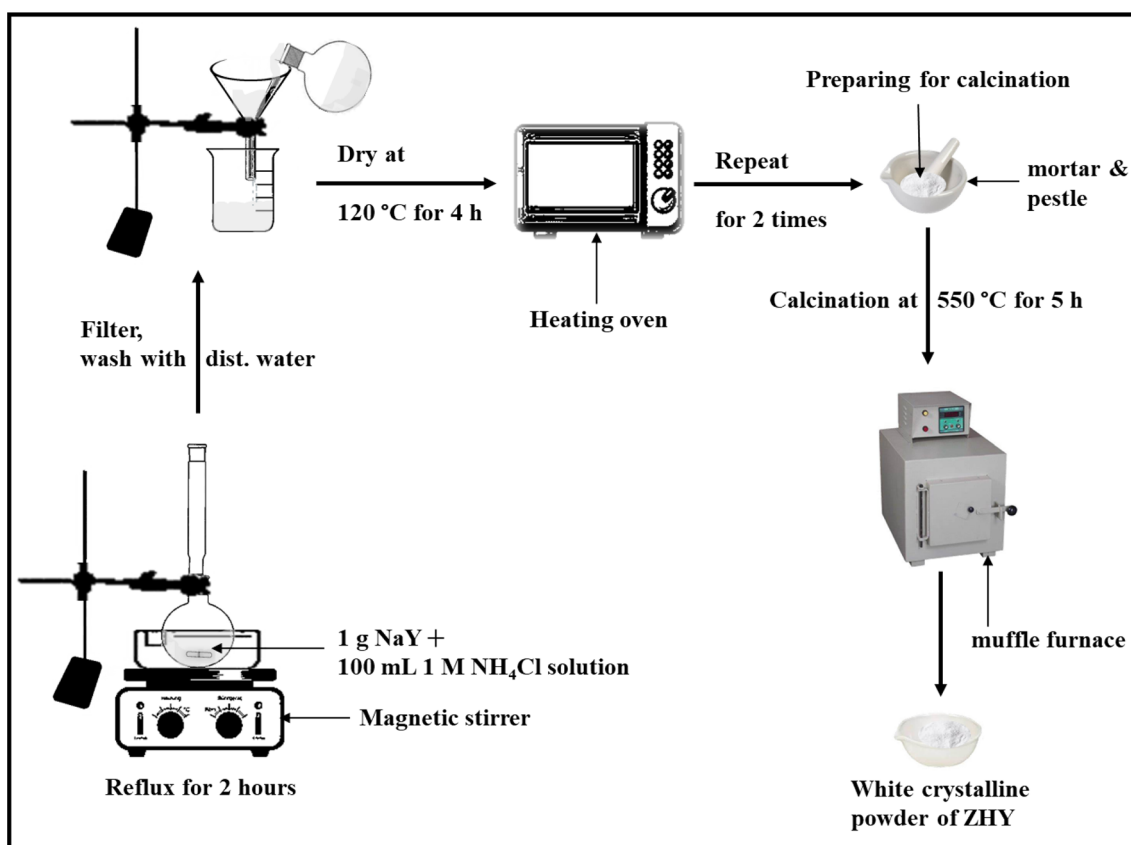
Zeolite NaY was converted into its protonic form HY by the conventional ion exchange method earlier reported by our group [24]. Scheme 2 represents the sequential steps involved to obtain ZHY.

Step II: Synthesis of mono lacunary phosphotungstate (PW_{11}).

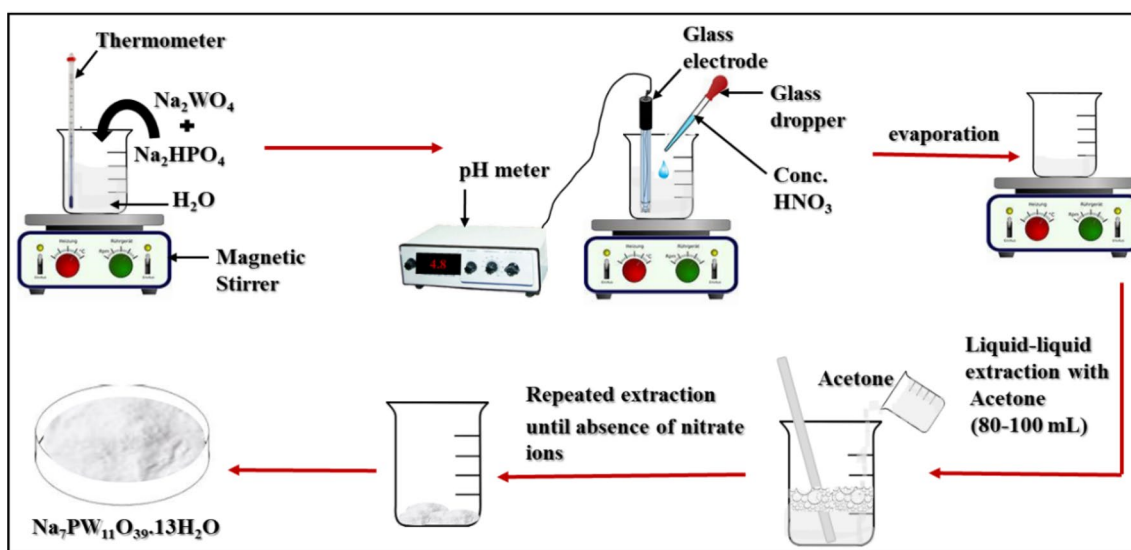
Sodium salt of PW_{11} ($Na_7PW_{11}O_{39} \cdot 13H_2O$) was synthesized by following the method reported by our group [5], in which sodium tungstate dihydrate (0.22 mol, 72.5 g) and anhydrous disodium hydrogen phosphate (0.02 mol, 2.84 g) were dissolved in 150–200 mL of conductivity water. Then, the solution was heated at 80–90 °C. After that, the pH was adjusted to 4.8 by adding concentrated HNO_3 followed by a liquid–liquid extraction of acetone to isolate the heteropoly anion after the volume was decreased by evaporation to half. The extraction was repeated until the absence of nitrate ions. The extracted sodium salt was dried in the air which further designated as PW_{11} . (Scheme 3) (Yield = 85–90%).

Step III: Anchoring of PW_{11} to ZHY.

Synthesis of a series of catalysts comprising 10–40 weight % of PW_{11} was carried out by the incipient wet impregnation method. 1 g of zeolite HY was suspended in an aqueous solution of PW_{11} (0.1 g/10 mL to 0.4/40 mL



Scheme 2 Ion exchange procedure for the conversion of NaY to ZHY



Scheme 3 Synthesis of PW₁₁

in distilled water). After stirring it for 5 h, the suspension was allowed to dry in the oven at 100 °C for 8 h. Afterwards, for complete drying put it for drying for 10 h. The obtained material was treated with 0.1 N HCl to exchange

the Na⁺ ions and then filtered, washed with distilled water, and dried at 100 °C. The obtained catalysts were designated as (PW₁₁)₁/ZHY, (PW₁₁)₂/ZHY, (PW₁₁)₃/ZHY and (PW₁₁)₄/ZHY respectively.

2.3 Characterization

2.3.1 Acidity Measurements

1) Total acidity by n-butylamine titration. In this method, a 0.025 M solution of n-butylamine in Toluene as well as 0.025 M Trichloroacetic acid (TCA) in Toluene was prepared [25]. The 0.25 g material was allowed for suspension in 25 mL n-butylamine solution for 24 h and the excess base was titrated against Trichloroacetic acid using neutral red as an indicator. Total acidity was calculated by given formula:

Calculation for Acidity

After titration, Volume of Blank, $V_{\text{blank}} = X$ ml.

Volume of Actual = Y ml.

Therefore, $V_{\text{used}} = X - Y = Z$ ml.

1000 ml 1 M TCA = 73.13 gm n-BA.

Z ml 0.025 M TCA = ?

$= Z * 0.025 * 73.13 / 1000 = A$ gm n-BA.

$1 * A / 0.25 = B$ gm n-BA.

Acidity (mmol/gm) = mole/ gm = B gm of n-BA/molecular weight of n-BA.

2) The total acidic sites as well as types of acidic sites were determined by potentiometric titration by using a DIGITAL pH METER DP 505 and pH/ Redox electrode & Conductivity Sensor (TOSHCON). In which, a suspension of 0.25 g of material was prepared in 25 mL of Acetonitrile and put in for stirring for about 12–15 min and initial electrode potential was measured (which indicates its acidic strength). A 0.05 N n-Butylamine (n-BA) solution in Acetonitrile (0.1 mL) was added to this suspension and allowed to stir for 3 h at 25 °C. Then potentiometrically, it was titrated against the same solution of n-Butylamine and the variation in electrode potential was noted with a digital pH meter. The acidic sites were calculated according to the following scale: $E_i > 100$ mV (very strong sites), $0 < E_i < 100$ mV (strong sites), $-100 < E_i < 0$ mV (weak sites) and $E_i < -100$ mV (very weak sites) [26].

2.3.2 Physicochemical Techniques

The BET (Brunauer–Emmett–Teller) surface area measurements as well as the N_2 adsorption–desorption isotherms (at 77 K) were recorded using Micromeritics ASAP 2010 (USA) volumetric static adsorption instrument. By using the BJH adsorption–desorption method, pore size distributions were calculated. For the elemental analysis, the JSM-7100F EDX-SEM analyser was used. The Mettler Toledo Star SW 7.01 was used under the nitrogen atmosphere for thermogravimetric analysis (TGA) with a flow rate of 2 mL min^{-1} at 25–600 °C (ramp rate of 10 °C min^{-1}). The Fourier Transform Infrared (FT-IR) spectra were recorded in the range 4000–400 cm^{-1} by using a KBr disc on a Shimadzu instrument (IRAffinity-1S). The Powder X-ray diffraction (XRD) patterns for the samples

were recorded using a Philips PW-1830 instrument in the 2 θ range 5–90° (Cu $K\alpha$ radiation $\lambda = 1.54 \text{ \AA}$). High resolution Transmission electron microscopy (HRTEM) was done by coating the samples on the Cu grid and scanned on a JEOL TEM instrument (model-JEM 2100) (JAPAN) with an acceleration voltage of 300 kV using carbon-coated 200 mesh.

2.4 Catalytic Activity

Esterification of levulinic acid and succinic acid with n-butanol were carried out in a 50 mL batch reactor. In which, acid (10 mmol), n-butanol (20 mmol or 30 mmol), and the catalyst were added and it was equipped with an air condenser, guard tube, and magnetic stirrer. With continuous stirring, the reaction mixture was heated at desired temperature and time. After completion of the reaction, the reaction mixture was cooled to room temperature and diluted with 15 mL of Dichloromethane (DCM) or methanol and centrifugation was carried out. Further, the reactants and products were analysed by a gas chromatograph GC-FID (Shimadzu-2014) using a capillary column RTX-5 (internal diameter:0.25 mm, length:30 m). The GC temperature profile for identification of n-butyl levulinate is as follows: The initial temperature was 35 °C, which was increased up to 300 °C. The hold time for ramp rate was initially 2 min at 80 °C (equilibration time=1.0 min) and then the rate increased by 10 up to 300 °C with a hold time of 6 min. For that, pressure = 100 kPa, total flow = 50.0 ml/min, column flow = 1.19 ml/min, linear velocity = 31.1 cm/sec and purge flow = 3.0 ml/min, were maintained. Likewise, for the identification of butyl succinates the following GC programming was applied: The temperature range was same as above (35 to 300 °C). The hold time for ramp rate was initially 2 min at 80 °C (equilibration time = 1.0 min) and then the rate increased by 25 up to 300 °C with a hold time of 5 min. These parameters, pressure = 69.4 kPa, total flow = 10.1 ml/min, column flow = 0.74 ml/min, linear velocity = 21.9 cm/sec and purge flow = 3.0 ml/min, were kept on for the same. The %conversion was calculated on the basis of acid. During the optimization of different main reaction parameters were performed thrice and the results were found to be reproducible with an error of $\pm 1\%$. The calculation for % conversion and % selectivity was obtained by the formulae given below.

$$\text{Conversion} = \frac{\text{initial mol} - \text{final mol}}{\text{initial mol}} \times 100$$

$$\text{Selectivity} = \frac{\text{moles of product formed}}{\text{moles of substrate consumed}} \times 100$$

2.5 Leaching and Hot Filtration Test

The leaching test of active species from the support was carried out by following the same procedure as in literature [27]. Qualitative determination of heteropoly acids can be studied by treating it with a mild reducing agent such as ascorbic acid, giving heteropoly blue coloration. 1 g of synthesized catalyst was suspended and kept in 10 mL water for 24 h. Then, the supernatant solution was decanted and treated with an ascorbic acid solution. As a result, no blue coloration was observed which specifies the absence of leaching of active species, PW₁₁ from the ZHY. Another method to find out the leaching of active species is a hot filtration test. It was checked through the residue obtained after the reaction. After the completion of the reaction, the reaction mass was filtered hot and the obtained filtrate was treated with the solution of ascorbic acid. The absence of blue colour indicates no leaching of PW₁₁ from ZHY.

3 Results and Discussion

3.1 Characterization

The results obtained by the elemental analysis of PW₁₁ presented in Table 1, which are quite in a good agreement with the calculated values [5]. These values indicate the successful formation of PW₁₁.

Further, to ensure the lacuna formation, FT-IR was carried out for PW₁₂ (Parent) as well as PW₁₁ (Fig. 1). By creating a defect in a parent species i.e., PW₁₂, a sharp split in the P-O stretching is observed. The observed P-O stretching at 1086 and 1043 cm⁻¹ is mainly due to the lowering of the symmetry from Td (PW₁₂) to Cs (PW₁₁) around the central heteroatom [29] which indicates the successful formation of lacuna. Bands at 863 and 808 cm⁻¹ correspond to W-O-W asymmetric stretching, while W=O stretching was observed at 952 cm⁻¹.

The total acidity of the support and catalyst was determined by n-butylamine titration and the results obtained are shown in Table 2. After the anchoring of active species into the support by impregnation, an increase in acidity was

Table 1 Elemental analysis of PW₁₁

Elements present in PW ₁₁	Calculated	Found by elemental analysis
W	65.2	65.8
P	0.99	1.01
O	27.5	27.9
Na	5.4	5.2

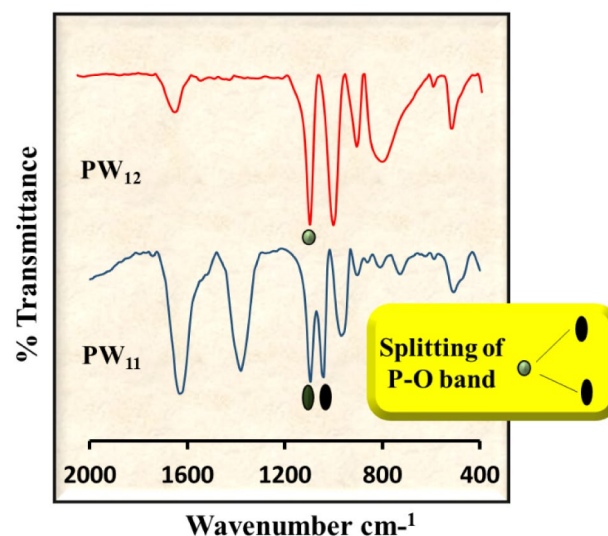


Fig. 1 FT-IR: Formation of mono lacunary from the parent phosphotungstates

observed, which shows successful impregnation of active species into the pores of support. The Bronsted acidity present in PW₁₁ is responsible for the increment of acidity. However, only a slight decrease in the same was observed when the % loading was increased further to 40%. This is due to the blocking of pores on the surface for the active sites. Hence, 30% loading was chosen as optimal here. Further, the results were correlated with the potentiometric titration method in which the acidic strength as well as acidic sites of support and catalyst were calculated. The results obtained are shown in Table 2. The change in electrode potential is observed as a function of mEq per gram of n-butylamine. ZHY shows an acidic nature, having an acidic strength of 289 mV and total acidic sites of 3.3 meqg⁻¹. Here again, by increasing the % loading of PW₁₁ from 10 to 30%, the significant increase was observed in the acidic strength (425–452 mV) as well as in the total acidic sites (4.5–6.8 meqg⁻¹) (Supplementary figure S1). The trend is same for both the titration methods. Once again, 30% was optimized. (PW₁₁)₃/ZHY was selected for further study and renamed PW₁₁/ZHY.

Textural properties of support and catalyst are presented in Table 3. PW₁₁/ZHY exhibits lower surface area than ZHY. It gives the first indication of sufficient anchoring of active species inside the pores of support. The same is said for an increase in pore diameter as well as pore volume.

Figure 2 depicts the nitrogen adsorption–desorption isotherm of both the support and catalyst. In which, ZHY exhibits a type-I isotherm with a hysteresis loop of H1 type that has cylindrical pores [28]. Note, these are the characteristics of the microporous material. PW₁₁/ZHY gives an identical isotherm with that of the ZHY which

Table 2 Acidity measurements of support and catalysts

Support/Catalysts	Potentiometric titration				n-Butylamine titration		
	Acidic Strength (mV)	Types of Acidic Sites (meqg ⁻¹)			Total No of Acidic Sites (meqg ⁻¹)	Total No of Acidic Sites (mmolg ⁻¹)	Total acidity (mmolg ⁻¹)
		Very Strong	Strong	Weak			
ZHY	289	0.4	0.4	2.5	3.3	0.66	0.83
(PW ₁₁) ₁ /ZHY	425	2.5	1.9	1.0	4.5	0.9	0.93
(PW ₁₁) ₂ /ZHY	440	2.9	2.0	1.2	5.3	1.06	1.13
(PW ₁₁) ₃ /ZHY	452	3.1	2.4	1.3	6.8	1.36	1.33
(PW ₁₁) ₄ /ZHY	450	3.0	1.6	1.4	6.0	1.20	1.30

Table 3 Textural properties of ZHY and PW₁₁/ZHY

Support/Catalyst	Surface area (m ² /g)	Pore diameter (Å)	Pore Volume (cm ³ /g)
ZHY	560	20.8	0.034
PW ₁₁ /ZHY	224	22.7	0.029

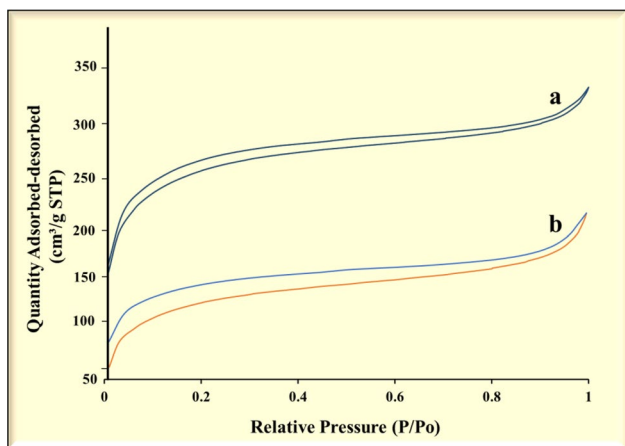


Fig. 2 N₂ adsorption–desorption isotherms of **a** ZHY and **b** PW₁₁/ZHY

Table 4 Elemental analysis of PW₁₁/ZHY by EDX

Material	Si (wt%)	O (wt%)	Al (wt%)	P (wt%)		W (wt%)	
				By EDX	Theoretical	By EDX	Theoretical
PW ₁₁ /ZHY	21.24	53.56	7.41	0.25	0.26	17.38	17.43

shows intact basic structure and successful anchoring of PW₁₁ into the pores of ZHY.

Table 4 shows the results of elemental analysis, and Fig. 3 presents its EDX mapping. The results are in good agreement with that the theoretical values which indicate the successful impregnation of PW₁₁.

The thermogravimetric analysis of ZHY shows weight loss in three steps. The very first weight loss of 20% corresponds to dehydration of the water adsorbed physically or chemically, in a temperature range between 60 and 150 °. Second weight loss was observed in a temperature range of 150–250 °C and that was 6.01%, which lead to the elimination of water molecules produced by the dehydroxylation of silicate and aluminium [24]. The last weight loss of 3.63% showed the possibility of some impurities. Further, its stability was observed up to 550 °C. Figure 4 shows the TGA of PW₁₁ and PW₁₁/ZHY. TGA of PW₁₁ shows a total weight loss of 11.04% in which initial weight loss of 7.3% in the temperature range of 60 to 230 °C is assigned to the loss of crystalline water, whereas the second weight loss of 3.74% corresponds to the distortion in the lacunary structure. TGA of PW₁₁/ZHY shows weight loss in two steps. Due to the loss of physically adsorbed water molecules, the initial weight loss of 19.88% was observed in the temperature range between 60 and 230 °C. After that, the final weight loss of 3.19% up to 560 °C was observed with the loss of

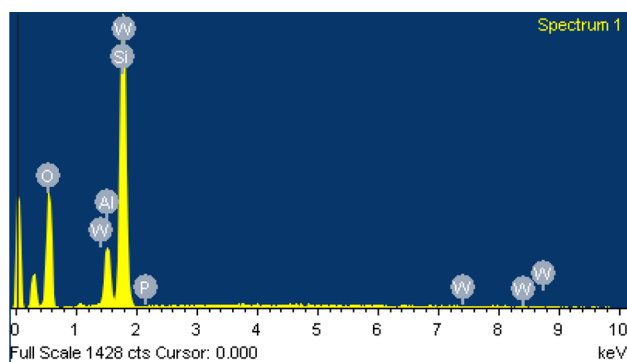


Fig. 3 EDX mapping of PW_{11}/ZHY

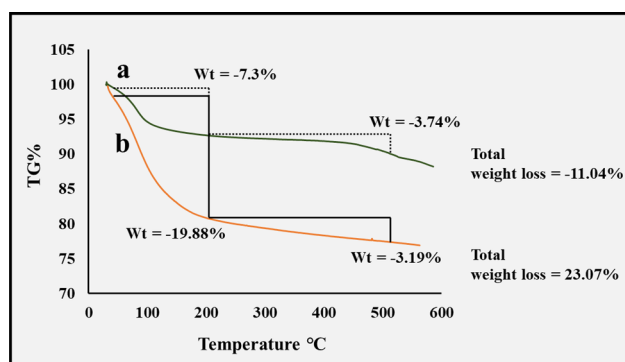


Fig. 4 TGA plots of **a** PW_{11} and **b** PW_{11}/ZHY

crystalline water molecules present in the Keggin unit. No further weight loss indicates the stability of the catalyst at higher temperatures.

FT-IR spectra of PW_{11} , ZHY, and PW_{11}/ZHY are shown in Fig. 5 FT-IR spectrum of ZHY shows broadband in the region of 3433 cm^{-1} which is attributed to the hydroxyl group of Si-OH bonds. The most intense bands of ZHY were located at about 1145 cm^{-1} and 1057 cm^{-1} corresponding to the internal Si-O(Si) and Si-O(Al) asymmetric stretching vibrations respectively of primary structural units, i.e., SiO_4 and AlO_4 tetrahedra. The bands at 785 and 578 cm^{-1} confirm symmetric stretching vibrations of Si-O-Si or Si-O-Al bridges, respectively [24]. The absence of bands at 1086 and 952 cm^{-1} in the FT-IR of PW_{11}/ZHY indicates the superimposition with that of the bands of ZHY. Typical bands such as PW_{11} , at 1054, 795, and 776 cm^{-1} show that the primary structure of the Keggin unit is preserved even after impregnation on ZHY. Here, the change in intensity was observed due to strong interaction between the lacunary Keggin unit and silanol groups of the support.

The Powder XRD patterns for PW_{11} , ZHY, and PW_{11}/ZHY are shown in Fig. 6. ZHY showed intense reflections at $2\theta = 6.55^\circ, 10.3^\circ, 11.3^\circ, 15.8^\circ, 17.6^\circ, \text{ and } 23.7^\circ$; 27.7°

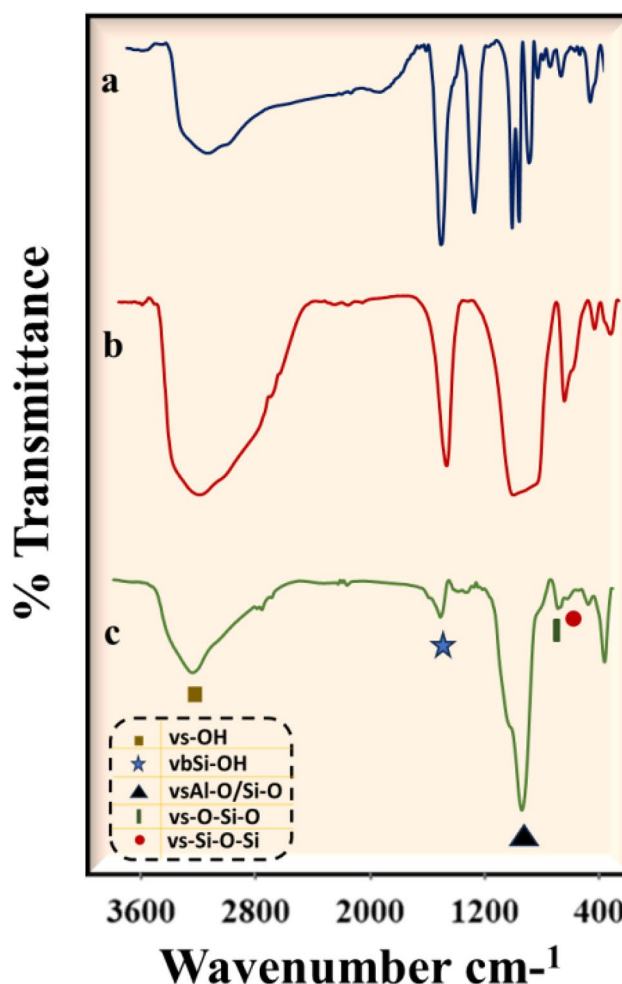


Fig. 5 FT-IR spectra of **a** PW_{11} , **b** ZHY and **c** PW_{11}/ZHY

corresponds to (111), (220), (311), (331), (511), (533), and (553) planes [30]. The X-ray diffraction pattern of PW_{11}/ZHY followed a similar pattern as that of ZHY which showed the intact zeolite structure even after introducing the active species. However, the observed decrease in the characteristic peaks is assigned to the fact that, after impregnation, the active species may reduce the scattering contrast between pore walls and pore spaces. The absence of characteristic peaks of PW_{11} suggests the good dispersion of PW_{11} inside the pores of ZHY.

Figure 7 displays the HRTEM images of ZHY and PW_{11}/ZHY at different magnifications. Figure a, b shows uniform dispersion of pores in ZHY. The hexagonal crystalline shape having a long-range ordered zeolite crystallinity which is observed through the material as long parallel crystallographic planes [31]. From the HRTEM images of PW_{11}/ZHY (Figure c, d), it is visible that the PW_{11} species are well dispersed through pores of ZHY and importantly, which shows that the lacunary structure is retained.

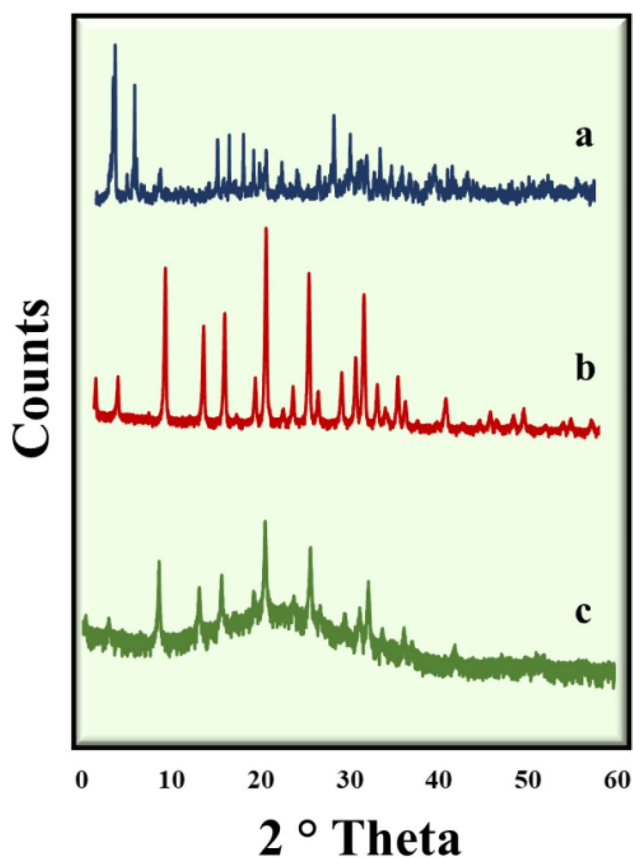


Fig. 6 XRD patterns of a PW_{11} , b ZHY and c PW_{11}/ZHY

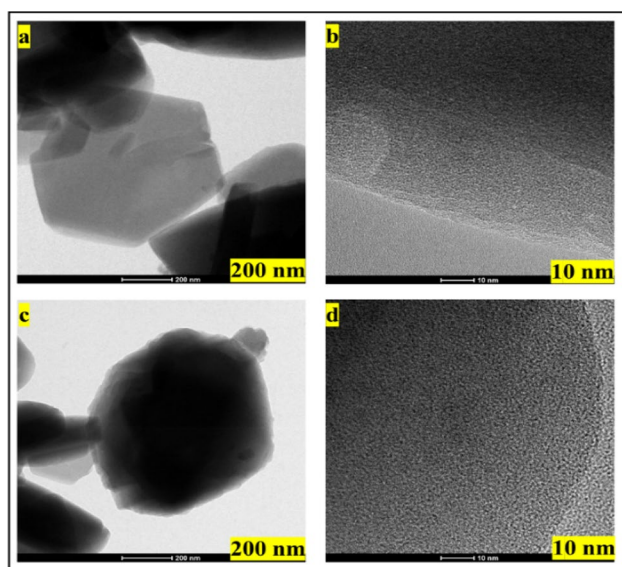


Fig. 7 HRTEM images of a, b ZHY and c, d PW_{11}/ZHY

3.2 Catalytic Performance

3.2.1 Levulinic Acid Esterification with n-Butanol

The general scheme of the esterification of levulinic acid with n-butanol using PW_{11}/ZHY to produce n-butyl levulinate is presented in Scheme 4.

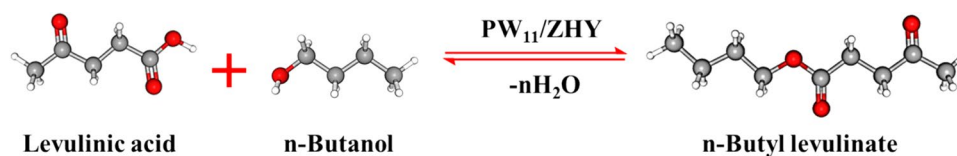
The effect of different parameters including the effect of loading amount of PW_{11} , the mole ratio of reactants, temperature, catalyst amount, and time was evaluated to get the maximum % conversion of n-butyl levulinate. The selectivity of product given here is of n-butyl levulinate, the intermediate here formed is pseudo butyl levulinate. The GC profiles for levulinic acid and product standard (n-butyl levulinate) and from that, GC profile of optimized conditions is also given in Supplementary figure S2.

The % loading of PW_{11} ranging from 10 to 40% (Table 5) shows an increase in the conversion as well as selectivity up to 30% loading which may be due to the fact that, more amount of PW_{11} will have more acidic sites. Later on, the trend reverses with further increase in % loading, and the conversion dropped down. The reason behind the decreased conversion is the blocking of catalytic active sites, as the excess catalytic active sites will increase the viscosity of the reaction mixture [32]. Hence, 30% loading was selected for the maximum conversion as well as selectivity. Further, all the reaction were carried out by taking 30% PW_{11}/ZHY and accordingly the influence of the different parameters is presented in the Fig. 8. The effect of catalyst amount was investigated by using 25, 50, and 75 mg of catalyst amount (Fig. 8b). By using the lowest amount of catalyst, the reaction gave significant conversion as well as selectivity and also, there was no sharp change observed after increasing the catalyst amount. Further, excess use of catalyst amount showed the inverse trend which attributed to the fact that higher active sites present in the catalyst lead to hydrolysis and the reaction proceeds to reverse [33].

The study of the impact of time on the reaction is crucial in the reversible reaction and the obtained results are shown in Fig. 8c. As expected, with an increase in time the conversion as well as selectivity was increased substantially. Further, on prolonging the time, the reaction conquers equilibrium and the conversion was found to be decreased. This is attributed to the reversible nature of the reaction.

To restrict the progress of side reactions and achieve the favourable results, it is important to study the effect of molar ratio on the reaction [32]. Figure 8d shows the results obtained after examined the different molar ratio of levulinic acid to n-butanol. With increase in molar ratio, a significant increase in the conversion was observed. This happened because the tendency of the esterification process to reverse hydrolyse needs an excess of alcohol to push the equilibrium in the forward direction. But, further increase in the molar

Scheme 4 Catalytic performance of PW_{11}/ZHY in levulinic esterification with n-butanol



ratio led to increase a dilution in reaction media as well as it reduces a mass transfer which result to fall in conversion.

Another important parameter, a reaction temperature, which governs the reaction rate, its influence was studied and obtained results are depicted in Fig. 8e. A drastic rise in the conversion was observed by increasing a temperature. This leads to high collision occurred from high thermal energy and mass transfer rates which result in a high conversion rate. After 90 °C, no significant increase in the % conversion was observed.

From the above detailed study, these are the optimized conditions to achieve maximum % conversion and selectivity using PW_{11}/ZHY as a catalyst: Molar ratio of acid to alcohol 1:2, amount of catalyst 25 mg (Active amount = 5.77 mg), reaction temperature = 90 °C and reaction time = 12 h, Turnover number (TON) = 2749. ($TON = \frac{\text{number of moles of substrate reacted}}{\text{number of moles of catalyst}}$).

3.2.2 Succinic Acid Esterification with n-Butanol

Later on, PW_{11}/ZHY was investigated for the organic transformation of another bio platform molecule. Scheme 5 depicted the di-esterification of succinic acid with n-butanol using PW_{11}/ZHY to yield both mono and dibutyl succinates. A detailed optimization study was conducted by studying the influence of various reaction parameters, similarly to the previous section.

The feasibility of the reaction was checked first with the catalysts having different % loading amounts of PW_{11} . From the Fig. 9a it was observed that here also, 30% loaded

catalyst gave maximum conversion of succinic acid with diester (Dibutyl succinate) selectivity.

Further, experiments were conducted with varied ratios to examine the impact of the mole ratio (Fig. 9b). The acid conversion as well as production of the diester, both aided by increasing the molar ratio. It should be noted that too much alcohol can dilute the reaction mixture and prevent the second esterification from occurring.

Figure 9c shows the impact of the catalyst amount. The conversion of acid should rise as catalyst amount increases since there are more number of acidic sites available. However, in this case, lowest amount of catalyst was sufficient to obtain the highest conversion and selectivity. Beyond that, less acid conversion was observed, which could be explained by the rise in overall solid mass density at higher catalyst concentrations.

Similarly, the influence of temperature and time was studied (Fig. 9d, e). Both parameters are vital for the reaction to proceed successfully and to yield the selectivity of the diester formation. With elevated temperature, the conversion increases tremendously to fourfold at 90 °C. As the reaction is endothermic, higher temperature promotes molecular collisions as well as di-esterification. Likewise, the conversion hiked with increased time and beyond that, a prolonged time did not significantly contribute to the conversion rate as well as selectivity.

The optimized reaction conditions for maximum conversion of succinic acid (96%) and selectivity of diester (61%) are, mole ratio 1:3; catalyst amount 25 mg; temperature 90 °C and time 12 h. The TON was found to be 3427. The GC profile for the optimized conditions is given in the Supplementary figure S3.

Table 5 Effect of % loading of PW_{11}

% loading of PW_{11}	% Conversion	% Selectivity	
		%n-butyl levulinate	% pseudo butyl levulinate
10	43	80	20
20	53	88	12
30	65	93	07
40	61	92	08

Reaction conditions: Mole ratio: 1:2, Catalyst amount: 25 mg, Temperature: 90 °C, Time:8 h

3.3 Kinetics: Determination of Activation Energy (Ea)

Activation energy for esterification of levulinic acid as well as succinic acid with n-butanol:

At intervals of 4, 6, 8, 10, and 12 h, kinetic studies of levulinic esterification with n-butanol were conducted in a temperature range of 70–100 °C. The rate constant was calculated graphically ($1/a-x$ vs time) for each temperature, and found to follow the 2nd order (Table 6) in which the graph shows a straight line with R^2 values ≥ 0.95 (Fig. 10a). It is important to calculate activation energy for a particular system to check its trueness towards the chemical step. The

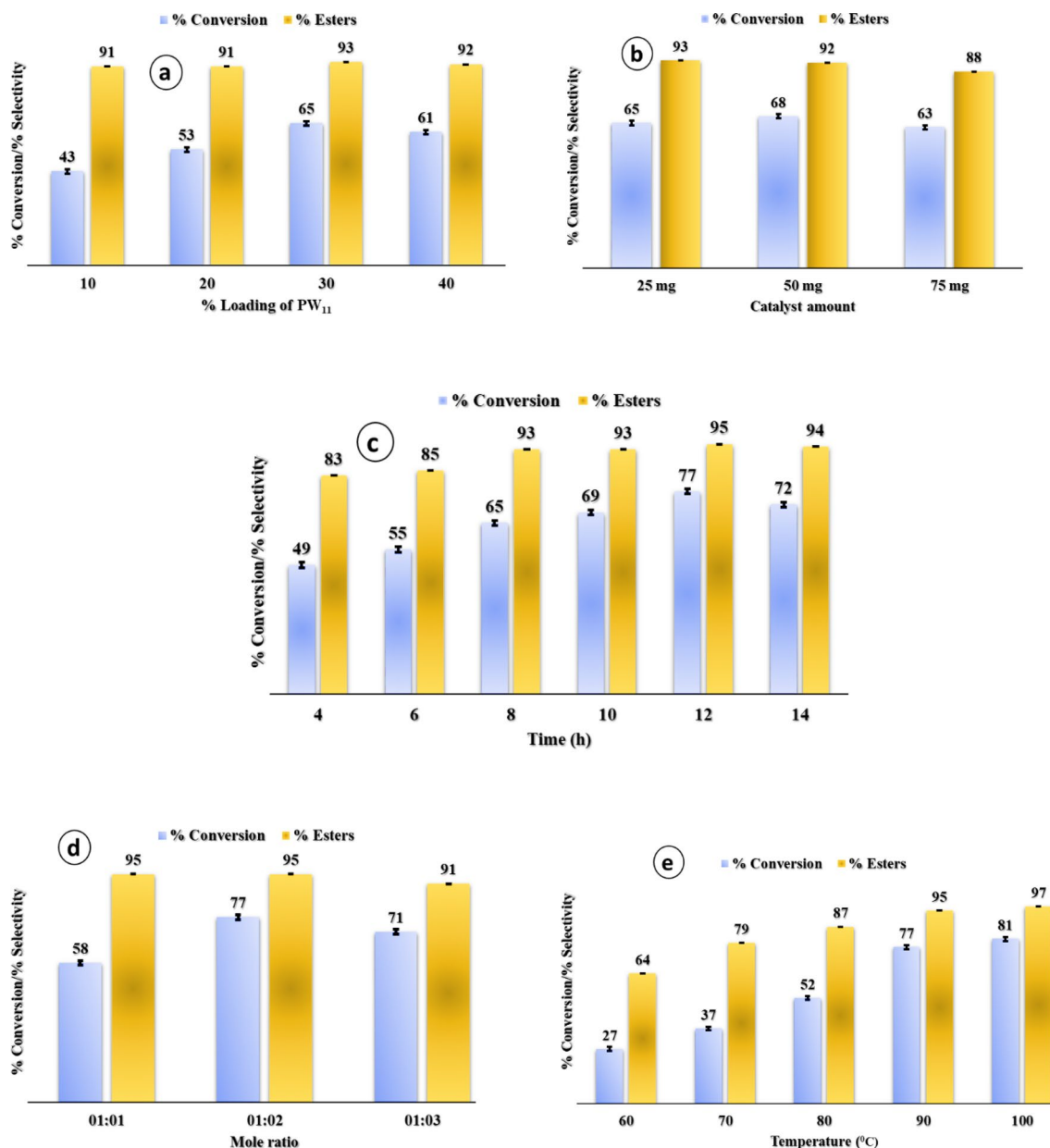


Fig. 8 **a** Effect of % loading of PW₁₁. Mole ratio: 1:2, Catalyst amount: 25 mg, Temperature: 90 °C, Time:8 h; **b** Effect of catalyst amount. Mole ratio: 1:2, Temperature:90 °C, Time: 8 h; **c** Effect of time. Mole ratio: 1:2, Catalyst amount: 25 mg, Temperature: 90 °C;

d Effect of mole ratio. Catalyst amount: 25 mg, Temperature: 90 °C, Time:12 h; **e** Effect of temperature. Mole ratio: 1:2, Catalyst amount: 25 mg, Time:12 h

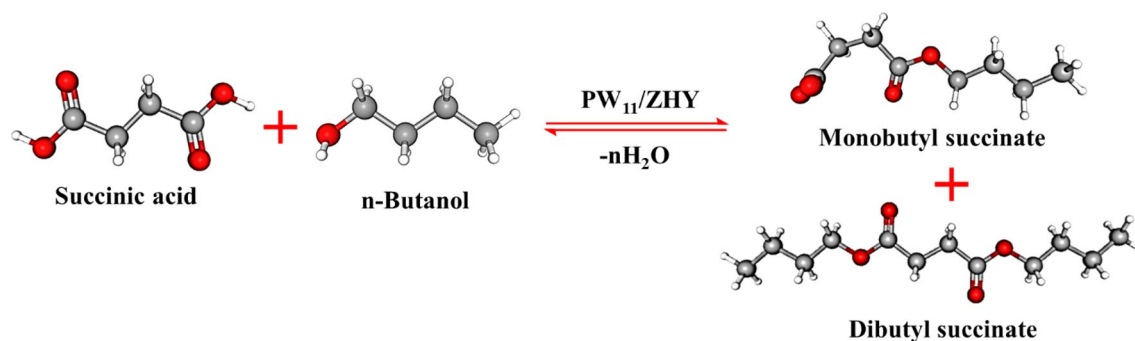
Fig. 10a also shows a graph of $\ln k$ vs $1/T$ and from that, the activation energy was calculated using the Arrhenius equation. It was found to be 88 kJ/mol.

Likewise, for succinic acid esterification, the graph of $1/(a-x)$ versus time (Fig. 10b) was plotted for different time intervals (6, 8, 10 and 12 h) at 70 to 100 °C, shows a linear relationship with respect to time confirming the second-order dependence of reaction. Table shows the rate constants at different temperatures and from that, the graph of $\ln k$

vs $1/T$ was plotted. The activation energy was found to be 127 kJ/mol.

A literature study says that if the activation energy exceeds 25 kJ/mol then the reaction is governed truly by chemical step [34]. In the present study, the activation energy for both the reactions is greater than 25 kJ/mol which confirms that the reactions are truly governed by a chemical step.

The order of the activation energy: Levulinic acid (88 kJ/mol) < Succinic acid (127 kJ/mol)]. This can be further



Scheme 5 Catalytic performance of $\text{PW}_{11}/\text{ZHY}$ in succinic esterification with n-butanol

justified as levulinic acid is a monocarboxylic keto acid, which means it only requires one acid group to convert into the desired ester. In contrast, succinic acid, which is a diacid, has two carboxylic acid groups, that requires more catalytic sites and a longer reaction time to undergo di-esterification in order to produce the desired diester. The obtained activation energy is in good agreement with this.

3.4 Control Experiments

For both reactions, control experiments using PW_{11} and ZHY alone were conducted and compared with those using the catalyst under optimized reaction conditions in order to understand the contribution of each species. From Table 7, it is visible that the conversion of both acids was found to be lower when ZHY alone was employed in the reactions than when PW_{11} was used alone. Whereas with the catalyst, significant conversion (77% of levulinic acid and 96% of succinic acid with 95% and 61% selectivity towards respective desired esters) which is higher compared to that of individual species was achieved.

These findings suggest that the Bronsted acidity of PW_{11} is a key factor which drives the reaction while, the β -cage like structure and geometry of ZHY will easily accommodate the reactant molecules and hence the esterification fits well. Hence, by combining the complementary properties of PW_{11} and ZHY, we were able to synthesize a heterogeneous catalyst that works really well in synergy to create the value-added products butyl levulinate and butyl succinate.

3.5 Regeneration and Recycling Studies

Studies on the regeneration and recycling of heterogeneous catalysts can be used to estimate the entire expense of production and feasibility. The catalyst was regenerated by using a simpler procedure. The reaction mixture was diluted with DCM (for levulinic acid esterification) or methanol (for

succinic acid esterification) after the first cycle, and the catalyst was separated by centrifugation method. The collected catalyst was further washed with fresh methanol, followed by water, and dried in an oven at 100 °C for approximately 2 h and employed for the next cycle. The regenerated catalyst is designated as R- $\text{PW}_{11}/\text{ZHY}$. Figure 11 displays the findings attained for both reactions which demonstrate the consistent activity of the catalyst up to 3 or 4 cycles. The recycling experiments thus confirm the sustainability of the catalyst by showing that the PW_{11} species does not leach from the ZHY and that it is stable enough to be used for numerous cycles.

3.6 Characterization of Regenerated Catalyst

The regenerated catalyst was characterized by acidity measurements, FT-IR and TGA.

The n-butylamine titration shows total acidity of the regenerated catalyst (1.32 mmol/g) was almost found to be like that of the fresh catalyst (1.33 mmol/g). From FT-IR analysis (Supplementary figure S4), the presence of all the characteristic bands of Keggin unit and that of the support indicates the stability and firm interaction of PW_{11} with ZHY. TGA analysis of regenerated catalyst shows very less change in the weight loss which may be attributed to the loss in catalyst amount in the recycling studies. (Table 8).

3.7 Relative Reactivity of Different Acids and Alcohols

$\text{PW}_{11}/\text{ZHY}$ was used to synthesize a variety of (industrially important) bio-based esters with a selectivity of 55–98% (Fig. 12). The figure depicted that the increase in carbon chain length of primary alcohols leads to an increase in % conversion. But there were controversial results in the case of methanol and ethanol as they have lower boiling points as compared to other primary alcohols. Therefore, the reaction was put in the pressure tube, while the remaining are in a batch reactor and so the results are different from the trend.

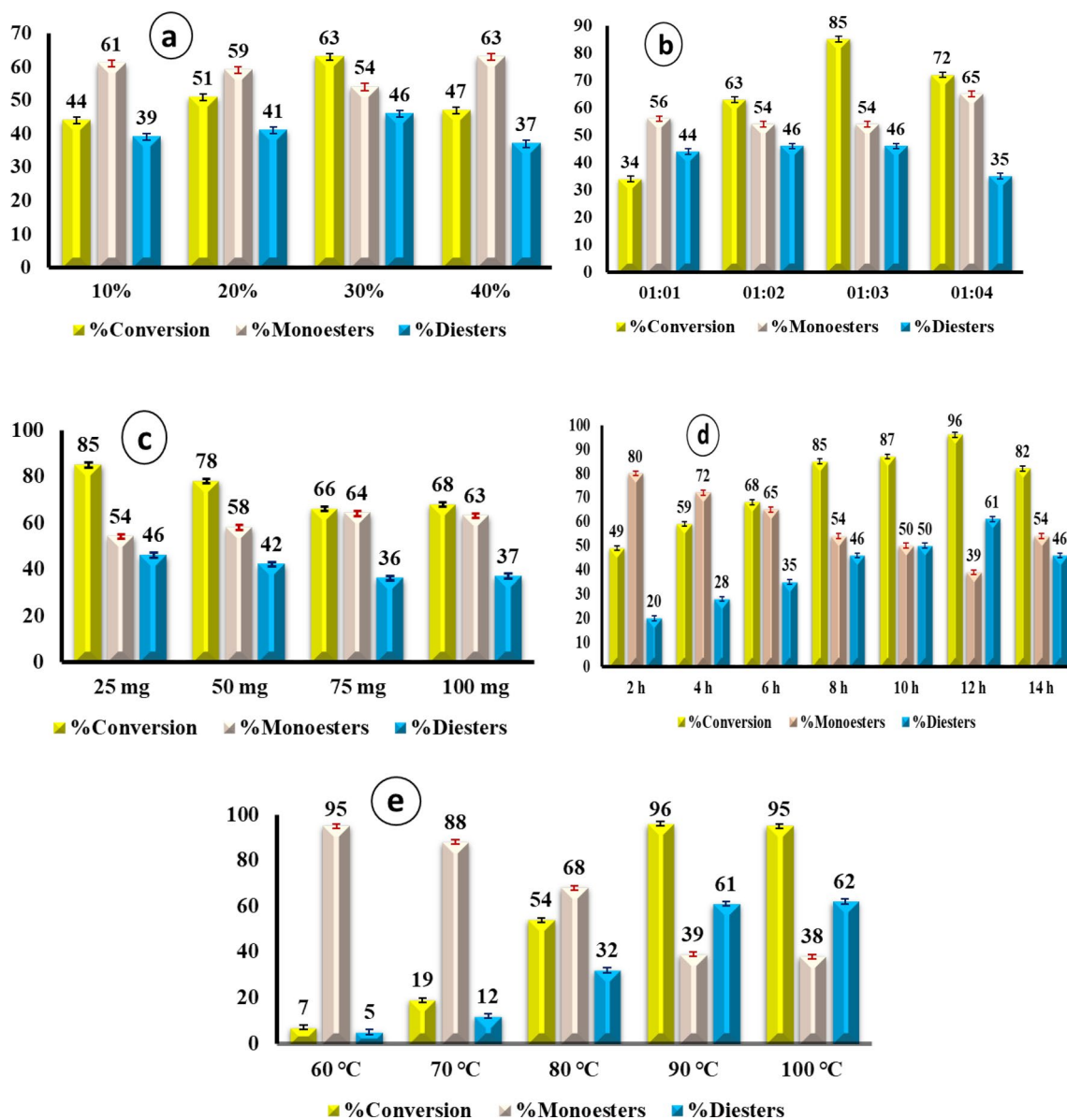


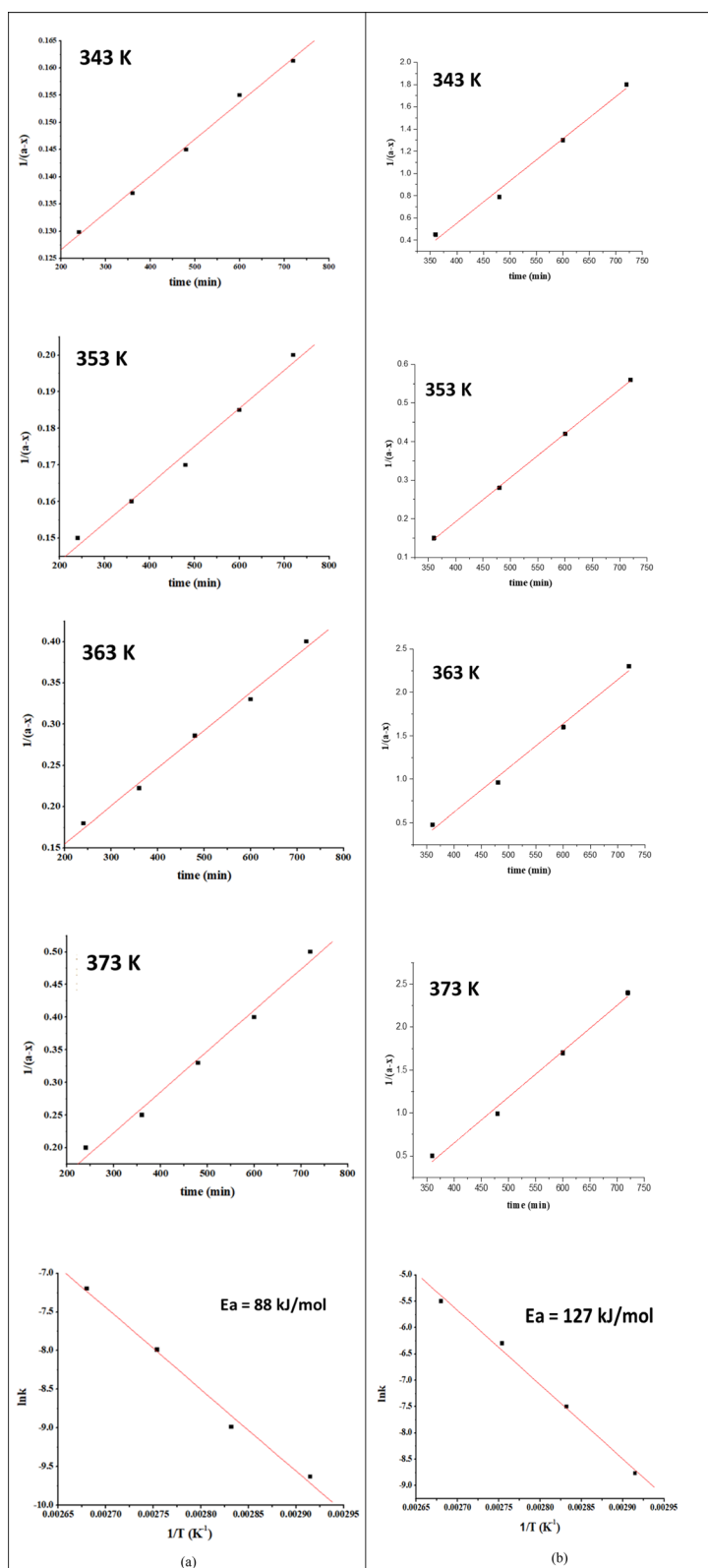
Fig. 9 a Effect of % loading of PW₁₁. Mole ratio: 1:2, Catalyst amount: 25 mg, Temperature: 90 °C, Time:8 h; **b**. Effect of mole ratio. Catalyst amount: 25 mg, Temperature: 90 °C, Time:12 h; **c** Effect of catalyst amount. Mole ratio: 1:3, Temperature:90 °C, Time:

8 h; **d** Effect of time. Mole ratio: 1:3, Catalyst amount: 25 mg, Temperature: 90 °C; **e** Effect of temperature. Mole ratio: 1:3, Catalyst amount: 25 mg, Time:12 h

Table 6 Rate constants ($M^{-1} \text{ min}^{-1}$), R^2 values at different temperatures and activation energy

Levulinic acid esterification				Succinic acid esterification			
Temp. (K)	Rate constant k ($M^{-1} \text{ min}^{-1}$)	R^2	Activation energy E_a (kJ/mol)	Temp. (K)	Rate constant k ($M^{-1} \text{ min}^{-1}$)	R^2	Activation energy E_a (kJ/mol)
343	6.57×10^{-5}	0.9958	88	343	6.88×10^{-5}	0.9898	127
353	1.25×10^{-4}	0.9889	$R^2=0.9987$	353	8.02×10^{-5}	0.9967	$R^2=0.9945$
363	3.71×10^{-4}	0.9933		363	1.26×10^{-4}	0.9950	
373	7.47×10^{-4}	0.9882		373	1.36×10^{-3}	0.9897	

Fig. 10 a Levulinic acid esterification Plots of $1/(a-x)$ vs Time (min) and Plot of $\ln k$ vs $1/T$
b Succinic acid esterification Plots of $1/(a-x)$ vs Time (min) and Plot of $\ln k$ vs $1/T$



Longer chain alcohols could be attributed to steric hindrance at the hydroxyl group of the alcohol, effectively allowing nucleophilic attack to the carbonyl carbon of the carboxylic

acid group of acid. Steric hindrance is known to slow down the reaction due to steric bulkiness, thereby blocking the access of the carboxylic acid to the esterification system.

Table 7 Control experiments

Catalyst/Support	Levulinic acid with n-butanol ^a		Succinic acid with n-butanol ^b	
	%Conversion	%Selectivity of esters	%Conversion	%Selectivity of diesters
¹ ZHY	56	93	60	39
² PW ₁₁	61	93	67	51
³ PW ₁₁ /ZHY	77	95	96	61

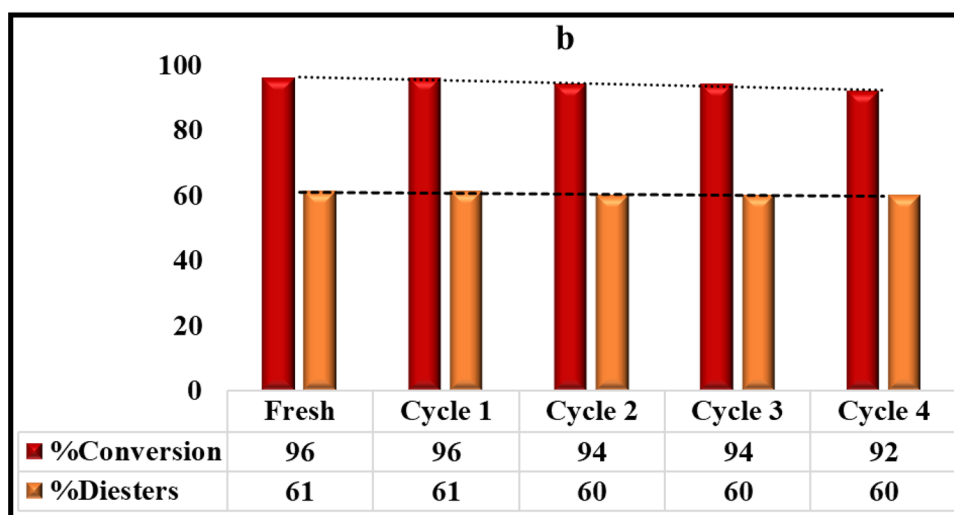
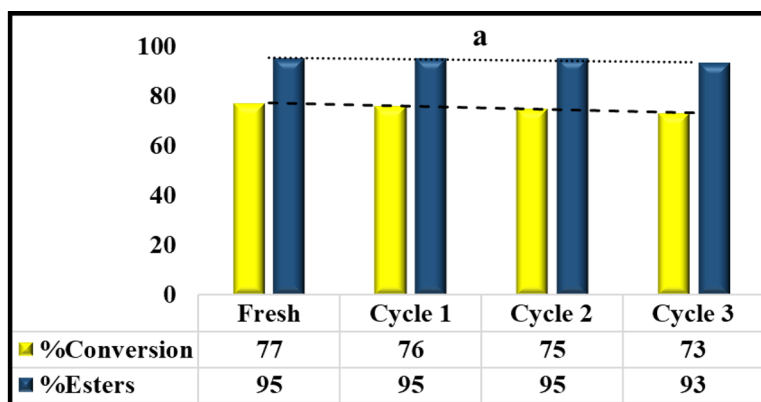
Reaction conditions: mole ratio: ^a1:2, ^b1:3; reaction temperature: ^a, ^b90 °C, reaction time: ^a, ^b12 h. Catalyst amount 1 = ^a, ^b19.23 mg, 2 = ^a, ^b 5.77 mg (active amount of PW₁₁), 3 = ^a, ^b 25 mg

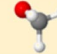
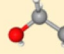
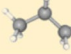
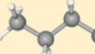
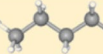
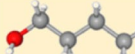
Steric hindrance can also be observed when molecules surrounding the active site unintentionally mask it due to their configuration. Steric hindrance also causes poor conversion to longer carbon chain length primary alcohols. This can be seen in the case of succinic acid esterification. However, in our case, we obtained controversial results for levulinic acid esterification. In which, the %conversion, as well as

selectivity of corresponding esters increase with increasing chain length. This could be attributed to electronic factors that promote stabilization of the formed carbocation intermediate to ester formation, despite the presence of steric hindrance. The esterification of both the acids with longer chain alcohols reflects very little literature. All the synthesized alkyl esters with carbon chain length up to C7 are worthy as they have a wide range of applications in industries. It is to be noted that, by varying the main reaction parameters the better results can be obtained for all the valuable bio-based esters. The catalysts, therefore, show remarkable reactivity towards the formation of the corresponding esters, exploring a versatile catalytic approach to acids.

Table 8 Textural properties of fresh and regenerated catalysts for TGA analysis

Catalyst	Total weight loss by TGA analysis
Fresh	23.07%
Regenerated	23.57%

Fig. 11 Recycling experiments for the esterification reaction of **a** Levulinic acid and **b** Succinic acid, with n-butanol in their optimized reaction conditions

%Conv.	%Esters	C1-C7 alcohols	%Conv.	%Diesters
45	94		61	65
62	95		74	61
60	93		89	56
64	92		92	64
73	95		88	59
77	98		84	55
Levulinic acid			Succinic acid	

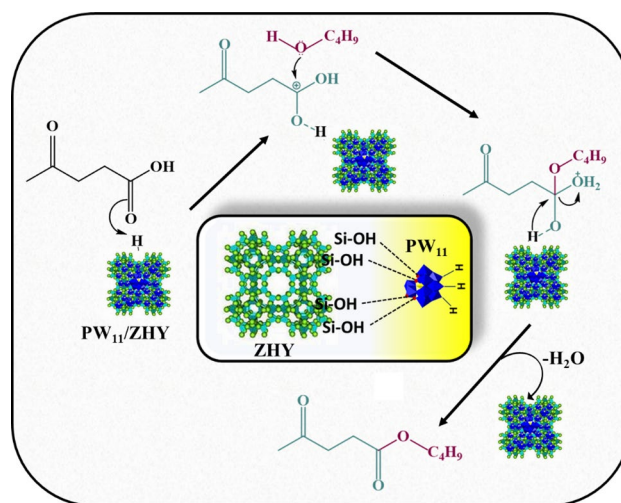
Note: Both the set of reactions were put in their optimized conditions

Fig. 12 Esterification of levulinic acid/succinic acid with different alcohols Note: Both the set of reactions were put in their optimized conditions

3.8 Reaction Mechanism

The reaction mechanism for the esterification of levulinic acid with n-butanol is previously reported by our group [27]. In the esterification of levulinic acid, an acid adsorption on the Brønsted acid sites of PW_{11}/ZHY leads to the formation of a protonated acid intermediate which will increase the electrophilicity of carbonyl carbon. Simultaneously, the carbonyl carbon is attacked by the nucleophilic oxygen of alcohol to form oxonium ion intermediate. After that, the tetrahedral intermediate loses a water molecule and produces n-butyl levulinate. The Brønsted acidity of PW_{11} as well as Lewis acid sites of ZHY plays a significant role in governing the reaction in a forward direction. Also, the activity of ZHY is related to the formation of the transition state inside the channels [24]. The available acidic sites of PW_{11}/ZHY promote the proton accessibility and favour the overall reaction (Scheme 6).

In the esterification of succinic acid, Both the monoester and diester will arise during the esterification of succinic acid and are anticipated to follow the same reaction process dependent on the competitive adsorption of alcohol and the acidity of the catalyst. The catalyst initially attracted the carbonyl group of succinic acid, which was then activated by the Brønsted acidic sites of PW_{11} . A protonated intermediate, as a result will function as an electrophile. Alcohol



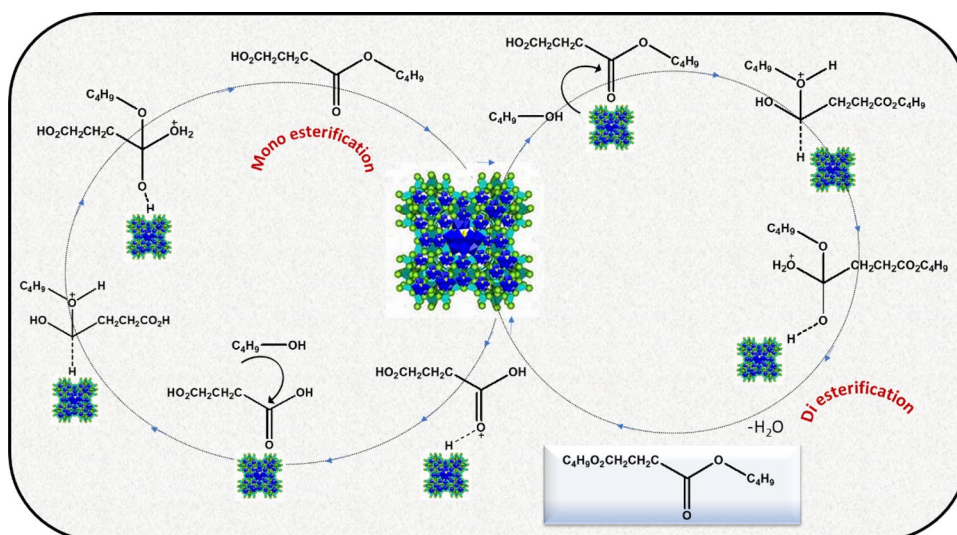
Scheme 6 Proposed mechanistic pathway for the levulinic esterification using PW_{11}/ZHY

acts as a nucleophile in this situation. This nucleophile will attack the carbonyl carbon that has been activated and produce a tetrahedral intermediate as a result. An intermediate is created when a water molecule is lost, and this mono butyl succinate is then desorbed. The formation of dibutyl succinate from the mono butyl succinate is the same. Because the present catalyst, PW_{11}/ZHY , offers more Brønsted acidic sites, more carboxylic acid groups can be activated, increasing diester formation and conversion. Because diesters are generated via Brønsted acidic sites [27] and ZHY is rich in Lewis acidity, mono-esterification is more likely to occur on this support (ZHY) than di-esterification (Scheme 7). This was also explained in the control experiments.

3.9 Comparison with Reported Catalytic Systems & Novelty of the Present Work

The present catalyst was compared to several successfully developed catalytic systems that produced butyl levulinates [35–40]. These systems were primarily impacted by harsh reaction conditions, specifically those exceeding 100 °C, high catalyst concentrations (~2 to 5% higher than the present catalyst), and high acid to alcohol molar ratios (between 2 and 5% higher than the present catalyst). Therefore, the superiority of the current catalyst is its ability to achieve noticeable activity under mild reaction conditions, such as 90 °C, with a small amount of catalyst usage, 25 mg and a molar ratio of 1:2. Concurrently, the activity of various known catalysts [27, 41–45] for the production of butyl succinates was compared. The present catalyst performs better here as well because it was employed at a lower temperature and with a smaller (2–19%) catalyst amount than previously reported. Additionally, the entire process is solvent-free and

Scheme 7 Proposed mechanistic pathway for the succinic esterification using PW_{11}/ZHY



hence does not require the use of solvents, unlike reported methods that use various solvents, which are not even considered as green chemicals, which diminishes the sustainability of the process.

In contrast to these systems, the current method operates at mild reaction conditions and most significantly, it is a solvent-free process. It was discovered, meanwhile, that no attempt has been made to employ lacunary phosphotungstate-based catalysts up until the date. For both of these conversions, the present catalyst is unique in its form. From the perspective of environmental and economic issues, the synthesis of butyl levulinate and butyl succinates is now more sustainable and greener when taking into account the aforementioned factors.

4 Conclusion

The successful synthesis via incipient wet impregnation of a novel sustainable heterogenous catalyst containing PW_{11} and ZHY was carried out. The detailed characterizations using variety of physicochemical techniques revealed the efficient synthesis of the mono lacunary species PW_{11} as well as its anchoring and interaction with ZHY. The catalyst demonstrated its promising activity by giving appreciable conversions of bio platform molecules to fuel additives, which falls under the performance of hexagonal channels of ZHY that easily accommodate the Bronsted acidity of PW_{11} that yields to maximum % conversion (77–96%) as well as selectivity of the desirable product (61–95%). The sustainability of the catalyst was found up to several cycles without significant loss of activity. In order to confirm the catalyst's adaptability, it was also used for the synthesis of other bio-based esters, which ultimately had a commercial impact. In a nutshell, the entire idea behind the present investigation is to develop

novel materials that are adept for offering sufficient energy sources to meet the globe's current energy needs.

Supplementary Information The online version contains supplementary material available at <https://doi.org/10.1007/s10562-024-04781-0>.

Acknowledgements AP and MJ are thankful to the Department of Chemistry, The Maharaja Sayajirao University of Baroda for the infrastructural facilities and DST-FIST for BET surface area analysis.

Author Contributions Anjali Patel: Conceptualization, Validation, Writing—Review & Editing, Visualization, Supervision. Margi Joshi: Methodology, Validation, Formal analysis, Investigation, Writing—Original draft.

Funding This research did not receive any specific grant from funding agencies in the public, commercial, or not-for profit sectors.

Data Availability Supplementary information is available.

Declarations

Conflict of interest There are no conflicts to declare.

References

- Misono M (1993) Catalytic chemistry of solid polyoxometalates and their industrial applications. *Mol Eng* 3:193–203. <https://doi.org/10.1007/BF00999633>
- Kozhevnikov IV (1998) Catalysis by heteropoly acids and multi-component polyoxometalates in liquid-phase reactions. *Chem Rev* 98:171–198. <https://doi.org/10.1021/cr960400y>
- Okuhara T, Mizuno N, Misono M. (1996) Catalytic Chemistry of Heteropoly Compounds. In: Eley DD, Haag WO, Gates BBT-A in C, editors. 41. Academic Press. 113–252. [https://doi.org/10.1016/S0360-0564\(08\)60041-3](https://doi.org/10.1016/S0360-0564(08)60041-3)
- Bellardita M, García-López EI, Marci G, Megna B, Pomilla FR, Palmisano L (2015) Photocatalytic conversion of glucose in aqueous suspensions of heteropolyacid-TiO₂ composites. *RSC Adv* 5:59037–59047. <https://doi.org/10.1039/C5RA09894G>

5. Singh S, Patel A (2015) Mono lacunary phosphotungstate anchored to MCM-41 as recyclable catalyst for biodiesel production via transesterification of waste cooking oil. *Fuel* 159:720–727. <https://doi.org/10.1016/j.fuel.2015.07.004>
6. Singh S, Patel A (2016) Environmentally benign oxidations of alkenes and alcohols to corresponding aldehydes over anchored phosphotungstates: effect of supports as well as oxidants. *Catal Lett* 146:1059–1072. <https://doi.org/10.1007/s10562-016-1732-7>
7. Patel A, Pathan S, Prakashan P (2016) One pot oxidative esterification of benzaldehyde over supported Cs-salt of mono nickel substituted phosphotungstate. *RSC Adv* 6:51394–51402. <https://doi.org/10.1039/C6RA04362C>
8. Wang H, Fang L, Yang Y, Hu R, Wang Y (2016) Immobilization $\text{Na}_7\text{PW}_{11}\text{O}_{39}$ on quaternary ammonium functionalized chloromethylated polystyrene by electrostatic interactions: an efficient recyclable catalyst for alcohol oxidation. *Appl Catal A*. <https://doi.org/10.1016/j.apcata.2016.03.034>
9. Koutsouroubi ED, Papadas IT, Armatas GS (2016) Ordered mesoporous polyoxometalate–organosilica frameworks as efficient photocatalysts of the hydrogen evolution. *ChemPlusChem*. <https://doi.org/10.1002/cplu.201600199>
10. Singh S, Patel A (2017) Value added products derived from biodiesel waste glycerol: activity, selectivity, kinetic and thermodynamic evaluation over anchored lacunary phosphotungstates. *J Porous Mater* 24:1409–1423. <https://doi.org/10.1007/s10934-017-0382-5>
11. Zeng G, Wu G, Wang Z, Li X, Yang, Zhang. 2021 Immobilization of $\text{K}_7\text{PW}_{11}\text{O}_{39}$ on ZrO_2 nanofiber ultra-deep desulfurization based in extraction catalytic oxidation desulfurization system. *Rev Chim*. 72: 89–101. <https://doi.org/10.37358/RC.21.3.8440>
12. Díaz J, Pizzio LR, Pecchi G, Campos CH, Azócar L, Briones R, Romero R, Henríquez A, Gaigneaux EM, Contreras D (2022) Tetrabutyl ammonium salts of kegg-in-type vanadium-substituted phosphomolybdates and phosphotungstates for selective aerobic catalytic oxidation of benzyl alcohol. *Catalysts* 12:507. <https://doi.org/10.3390/catal12050507>
13. Kato CN, Kubota T, Aono K, Ozawa N (2022) Two tungstates containing platinum nanoparticles prepared by air-calcining kegg-in-type polyoxotungstate-coordinated diplatinum (ii) complexes: effect on sintering-resistance and photocatalysis. *Catal Lett* 152:2553–2563. <https://doi.org/10.1007/s10562-021-03843-x>
14. Malmir M, Heravi MM, Ghasemi ZY, Mirzaei M (2022) Incorporating heterogeneous lacunary Keggin anions as efficient catalysts for solvent-free cyanosilylation of aldehydes and ketones. *Sci Rep* 12:11573. <https://doi.org/10.1038/s41598-022-15831-1>
15. Korenev VS, Abramov PA, Sokolov MN (2022) Azide coordination to polyoxometalates: synthesis of $(\text{Bu}_4\text{N})_{4.3}\text{K}_{0.7}[\text{PW}_{11}\text{O}_{39}\text{Fe}^{\text{III}}\text{N}_3] \cdot 2.5\text{H}_2\text{O}$. *Russ J Inorg Chem* 67:1763–1768. <https://doi.org/10.1134/S0036023622600897>
16. Jan R, Biji CA, Shakeela K, Shaikh RR, Rao GR (2023) Green synthesis of cyclic carbonates from epoxides and CO_2 using transition metal substituted polyoxometalate-PDDA hybrid catalysts. *Catal Lett*. <https://doi.org/10.1007/s10562-023-04392-1>
17. Korenev VS, Sukhikh TS, Sokolov MN (2023) A series of lanthanide complexes with kegg-in-type monolacunary phosphotungstate: synthesis and structural characterization. *Inorganics* 11:327. <https://doi.org/10.3390/inorganics11080327>
18. Xiao Q, Jiang Y, Yuan W, Chen J, Li H, Zheng H (2023) Styrene epoxidation catalyzed by polyoxometalate/quaternary ammonium phase transfer catalysts: the effect of cation size and catalyst deactivation mechanism. *Chin J Chem Eng* 55:192–201. <https://doi.org/10.1016/j.cjche.2022.04.024>
19. Haruna A, Merican ZMA, Musa SG (2023) Remarkable stability and catalytic performance of $\text{PW}_{11}\text{M}@\text{MOF}-808$ (M=Mn and Cu) nanocomposites for oxidative desulfurization of fuel oil. *Mol Catal* 541:113079. <https://doi.org/10.1016/j.mcat.2023.113079>
20. Krishnan V, McCalley JD (2016) The role of bio-renewables in national energy and transportation systems portfolio planning for low carbon economy. *Renew Energy* 91:207–223. <https://doi.org/10.1016/j.renene.2016.01.052>
21. Christensen E, Williams A, Paul S, Burton S, McCormick RL (2011) Properties and performance of levulinic esters as diesel blend components. *Energy Fuels* 25:5422–5428. <https://doi.org/10.1021/ef201229j>
22. Delhomme C, Weuster-Botz D, Kuhn FE (2009) Succinic acid from renewable resources as a C4 building-block chemical- a review of the catalytic possibilities in aqueous media. *Green Chem* 11:13–26. <https://doi.org/10.1039/B810684C>
23. Serrano-Ruiz JC, Luque R, Sepúlveda-Escribano A (2011) Transformations of biomass derived platform molecules: from high added-value chemicals to fuels via aqueous phase processing. *Chem Soc Rev* 40:5266–5281. <https://doi.org/10.1039/C1CS15131B>
24. Patel A, Joshi M, Sharma S (2022) Designing of a novel heterogeneous catalyst comprising 12-tungstophosphoric acid and zeolite HY for the synthesis of bio-based esters. *Biomass Conv Bioref*. <https://doi.org/10.1007/s13399-022-03279-2>
25. Sahu HR, Rao GR (2000) Characterization of combustion synthesized zirconia powder by UV- vis, IR and other techniques. *Bull Mater Sci* 23:349–354. <https://doi.org/10.1007/BF0270838339>
26. Ferreira P, Fonseca IM, Ramos AM, Vital J, Castanheiro JE (2010) Valorisation of glycerol by condensation with acetone over silica-included heteropolyacids. *Appl Catal B* 98:94–99. <https://doi.org/10.1016/j.apcatb.2010.05.018>
27. Pithadia D, Patel A (2023) Mono lacunary silicotungstate anchored to nano-porous MCM-48: synthesis, characterization and esterification of biplatform molecules to fuel additives. *J Ind Eng Chem* 119:236–251. <https://doi.org/10.1016/j.apcata.2020.117729>
28. Ramli NAS, Amin NAS (2014) Fe/HY zeolite as an effective catalyst for levulinic acid production from glucose: characterization and catalytic performance. *Appl Catal B* 163:487–498. <https://doi.org/10.1016/j.apcatb.2014.08.031>
29. Okuhara T, Mizuno N, Misono M (1996) Catalytic chemistry of heteropoly acid compounds. *Adv Catal* 41:113–252. [https://doi.org/10.1016/S0360-0564\(08\)60041-3](https://doi.org/10.1016/S0360-0564(08)60041-3)
30. Freitas EF, Araújo AAL, Paiva MF, Dias SCL, Dias JA (2018) Comparative acidity of BEA and Y zeolite composites with 12- tungstophosphoric and 12-tungstosilicic acids. *Mol Catal* 458:152–160. <https://doi.org/10.1016/j.mcat.2018.03.005>
31. Cui W, Zhu D, Tan J, Chen N, Fan D, Wang J, Han J, Wang L, Tian P, Liu Z (2022) Synthesis of mesoporous high-silica zeolite Y and their catalytic cracking performance. *Chin J Catal* 43:1945–1954. [https://doi.org/10.1016/S1872-2067\(21\)64043-3](https://doi.org/10.1016/S1872-2067(21)64043-3)
32. Badgujara KC, Badgujara VC, Bhanage BM (2020) A review on catalytic synthesis of energy rich fuel additive levulinic compounds from biomass derived levulinic acid. *Fuel Process Technol* 97:106213. <https://doi.org/10.1016/j.fuproc.2019.106213>
33. Schüth F, Ward MD, Buriak JM (2018) Common pitfalls of catalysis manuscripts submitted to chemistry of materials. *Chem Mater* 30:3599–3600. <https://doi.org/10.1021/acs.chemmater.8b01831>
34. Bond GC (1974) *Heterogeneous catalysis: principles and applications*. Clarendon Press, Oxford
35. Tian Y, Zhu X, Zhou S (2023) Efficient synthesis of alkyl levulinates fuel additives using sulfonic acid functionalized polystyrene coated coal fly ash catalyst. *J Biosour Bioprod* 8:198–213. <https://doi.org/10.1016/j.jobab.2023.01.003>
36. Zhou S, Wu L, Bai J et al (2022) Catalytic esterification of levulinic acid into the biofuel n-butyl levulinate over nanosized TiO_2 particles. *Nanomaterials* 12(3870):15. <https://doi.org/10.3390/nano12213870>

37. Zhou S, Long M, Wu L et al (2022) Titanate nanotubes covalently bonded sulfamic acid as a heterogeneous catalyst for highly efficient conversion of levulinic acid into n-butyl levulinate biofuels. *Biomass Convers Biorefin*. <https://doi.org/10.1007/s13399-022-03179-5>
38. Patel A, Morawala D, Lankapati H et al (2021) Ti-ATMP catalyzed esterification of levulinic acid to synthesize butyl ester. *Mater Today Proc*. <https://doi.org/10.1016/j.matpr.2021.01.347>
39. Pithadia D, Patel A, Hatiya V (2022) 12-Tungstophosphoric acid anchored to MCM-22, as a novel sustainable catalyst for the synthesis of potential biodiesel blend, levulinate ester. *Renew Energy* 187:933–943. <https://doi.org/10.1016/j.renene.2022.01.106>
40. Peixoto AF, Soliman MM, Pinto TV, Silva SM, Costa P, Alegria EC, Freire C (2021) Highly active organosulfonic aryl-silica nanoparticles as efficient catalysts for biomass derived biodiesel and fuel additives. *Biomass Bioenergy* 145:105936. <https://doi.org/10.1016/j.biombioe.2020.105936>
41. Leng Y, Wang J, Zhu D, Ren X, Ge H, Shen L (2009) Heteropolyanion-based ionic liquids: reaction-induced self-separation catalysts for esterification. *Angew Chem* 121:174–177. <https://doi.org/10.1002/anie.200803567>
42. Vijayakumar B, Nagendrappa G, Jai PB, S. (2009) Acid activated indian bentonite, an efficient catalyst for esterification of carboxylic acids. *Catal Lett* 128:183–189. <https://doi.org/10.1007/S10562-008-9729-5>
43. Leng Y, Jiang P, Wang. (2012) A novel Brønsted acidic heteropolyanion-based polymeric hybrid catalyst for esterification. *Catal Commun* 25:41–44. <https://doi.org/10.1016/j.catcom.2012.04.014>
44. Jing C., Jinhua L., Zhongxie D., Yuehua W., Zhen L., Min J., Xiaoqian R. (2018) Lewis acid sites of mg modified polystyrene sulfonic acid resin catalysis for synthesis of dibutyl succinate. *Química Nova*. 41: 613–618. <https://doi.org/10.21577/0100-4042.20170230>
45. Szelwicka A, Boncel S, Jurczyk S, Chrobok A (2019) Exceptionally active and reusable nanobiocatalyst comprising lipase non-covalently immobilized on multi-wall carbon nanotubes for the synthesis of diester plasticizers. *Appl Catal A Gen* 574:41–47. <https://doi.org/10.1016/j.apcata.2019.01.030>

Publisher's Note Springer Nature remains neutral with regard to jurisdictional claims in published maps and institutional affiliations.

Springer Nature or its licensor (e.g. a society or other partner) holds exclusive rights to this article under a publishing agreement with the author(s) or other rightsholder(s); author self-archiving of the accepted manuscript version of this article is solely governed by the terms of such publishing agreement and applicable law.

Authors and Affiliations

Anjali Patel¹  · Margi Joshi¹

✉ Anjali Patel
anjali.patel-chem@msubaroda.ac.in

¹ Polyoxometalates and Catalysis Laboratory, Department of Chemistry, Faculty of Science, The Maharaja Sayajirao University of Baroda, Vadodara 390020, Gujarat, India